

Dynamics of viscoplastic deformation in amorphous solids

M. L. Falk and J. S. Langer

Department of Physics, University of California, Santa Barbara, Santa Barbara, California 93106

(Received 11 December 1997)

We propose a dynamical theory of low-temperature shear deformation in amorphous solids. Our analysis is based on molecular-dynamics simulations of a two-dimensional, two-component noncrystalline system. These numerical simulations reveal behavior typical of metallic glasses and other viscoplastic materials, specifically, reversible elastic deformation at small applied stresses, irreversible plastic deformation at larger stresses, a stress threshold above which unbounded plastic flow occurs, and a strong dependence of the state of the system on the history of past deformations. Microscopic observations suggest that a dynamically complete description of the macroscopic state of this deforming body requires specifying, in addition to stress and strain, certain average features of a population of two-state shear transformation zones. Our introduction of these state variables into the constitutive equations for this system is an extension of earlier models of creep in metallic glasses. In the treatment presented here, we specialize to temperatures far below the glass transition and postulate that irreversible motions are governed by local entropic fluctuations in the volumes of the transformation zones. In most respects, our theory is in good quantitative agreement with the rich variety of phenomena seen in the simulations. [S1063-651X(98)01306-3]

PACS number(s): 83.50.Nj, 62.20.Fe, 61.43.-j, 81.05.Kf

I. INTRODUCTION

This paper is a preliminary report on a molecular-dynamics investigation of viscoplastic deformation in a non-crystalline solid. It is preliminary in the sense that we have completed only the initial stages of our planned simulation project. The results, however, have led us to a theoretical interpretation that we believe is potentially useful as a guide for further investigations along these lines. In what follows, we describe both the simulations and the theory.

Our original motivation for this project was an interest in the physics of deformations near the tips of rapidly advancing cracks, where materials are subject to very large stresses and experience very high strain rates. Understanding the dissipative dynamics that occur in the vicinity of the crack tip is necessary to construct a satisfactory theory of dynamic fracture [1]. Indeed, we believe that the problem of dynamic fracture cannot be separated from the problem of understanding the conditions under which a solid behaves in a brittle or ductile manner [2–6]. To undertake such a project we eventually shall need sharper definitions of the terms “brittle” and “ductile” than are presently available; but we leave such questions to future investigations while we focus on the specifics of deformation in the absence of a crack.

We have chosen to study amorphous materials because the best experiments on dynamic instabilities in fracture have been carried out in silica glasses and polymers [7,8]. We know that amorphous materials exhibit both brittle and ductile behavior, often in ways that, on a macroscopic level, look very similar to deformation in crystals [9]. More generally, we are looking for fundamental principles that might point us toward theories of deformation and failure in broad classes of macroscopically isotropic solids where thinking of deformation in terms of the dynamics of individual dislocations [2,3] is either suspect, due to the absence of underlying crystalline order, or simply intractable, due to the extreme complexity of such an undertaking. In this way we hope that the ideas presented here will be generalizable perhaps to

some polycrystalline materials or even single crystals with large numbers of randomly distributed dislocations.

We describe our numerical experiments in Sec. II. Our working material is a two-dimensional, two-component, non-crystalline solid in which the molecules interact via Lennard-Jones forces. We purposely maintain our system at a temperature very far below the glass transition. In the experiments, we subject this material to various sequences of pure shear stresses, during which we measure the mechanical response. The simulations reveal a rich variety of behaviors typical of metallic glasses [10–13] and other viscoplastic solids [14], specifically, reversible elastic deformation at small applied stresses, irreversible plastic deformation at somewhat larger stresses, a stress threshold above which unbounded plastic flow occurs, and a strong dependence of the state of the system on the history of past deformations. In addition, the molecular-dynamics method permits us to see what each molecule is doing at all times; thus we can identify the places where irreversible molecular rearrangements are occurring.

Our microscopic observations suggest that a dynamically complete description of the macroscopic state of this deforming body requires specifying, in addition to stress and strain, certain average features of a population of what we shall call “shear transformation zones.” These zones are small regions, perhaps consisting of only five or ten molecules, in special configurations that are particularly susceptible to inelastic rearrangements in response to shear stresses. We argue that the constitutive relations for a system of this kind must include equations of motion for the density and internal states of these zones; that is, we must add new time-dependent state variables to the dynamical description of this system [15,16]. Our picture of shear transformation zones is based on earlier versions of the same idea due to Argon, Spaepen, and others who described creep in metallic alloys in terms of activated transitions in intrinsically heterogeneous materials [17–22]. These theories, in turn, drew on previous free-volume formulations of the glass transition by

Turnbull, Cohen, and others in relating the transition rates to local free-volume fluctuations [20,23–25]. None of those theories, however, were meant to describe the low-temperature behavior seen here, especially the different kinds of irreversible deformations that occur below and above a stress threshold, and the history dependence of the response of the system to applied loads.

We present the theory of the dynamics of shear transformation zones in Sec. III. This theory contains four crucial features that are not, so far as we know, in any previous analysis. First, once a zone has transformed and relieved a certain amount of shear stress, it cannot transform again in the same direction. Thus the system saturates and, in the language of granular materials, it becomes “jammed.” Second, zones can be created and destroyed at rates proportional to the rate of irreversible plastic work being done on the system. This is the ingredient that produces a threshold for plastic flow; the system can become “unjammed” when new zones are being created as fast as existing zones are being transformed. Third, the attempt frequency is tied to the noise in the system, which is driven by the strain rate. The stochastic nature of these fluctuations is assumed to arise from random motions associated with the disorder in the system. Fourth, the transition rates are strongly sensitive to the applied stress. It is this sensitivity that produces memory effects.

The resulting theory accounts for many of the features of the deformation dynamics seen in our simulations. However, it is a mean-field theory that fails to take into account any spatial correlations induced by interactions between zones and therefore it cannot explain all aspects of the behavior that we observe. In particular, the mean-field nature of our theory precludes, at least for the moment, any analysis of strain localization or shear banding.

II. MOLECULAR-DYNAMICS EXPERIMENTS

A. Algorithm

Our numerical simulations have been performed in the spirit of previous investigations of deformation in amorphous solids [26–29]. We have examined the response to an applied shear of a noncrystalline, two-dimensional, two-component solid composed of either 10 000 or 20 000 molecules interacting via Lennard-Jones forces. Our molecular-dynamics algorithm is derived from a standard NPT (number, pressure, temperature) dynamics scheme [30], i.e., a pressure-temperature ensemble, with a Nose-Hoover thermostat [31–33] and a Parrinello-Rahman barostat [34,35] modified to allow imposition of an arbitrary two-dimensional stress tensor. The system obeys periodic boundary conditions and both the thermostat and barostat act uniformly throughout the sample.

Our equations of motion are

$$\dot{\mathbf{r}}_n = \frac{\mathbf{p}_n}{m_n} + [\dot{\varepsilon}] \cdot (\mathbf{r}_n - \mathbf{R}_0), \quad (2.1)$$

$$\dot{\mathbf{p}}_n = \mathbf{F}_n - ([\dot{\varepsilon}] + \xi[I])\mathbf{p}_n, \quad (2.2)$$

$$\dot{\xi} = \frac{1}{\tau_T^2} \left(\frac{T_{kin}}{T} - 1 \right), \quad (2.3)$$

$$[\dot{\varepsilon}] = -\frac{1}{\tau_p^2} \frac{V}{Nk_B T} ([\sigma_{av}] - [\sigma]), \quad (2.4)$$

$$\dot{\mathbf{L}} = [\dot{\varepsilon}] \cdot \mathbf{L}. \quad (2.5)$$

Here \mathbf{r}_n and \mathbf{p}_n are the position and momentum of the n th molecule and \mathbf{F}_n is the force exerted on that molecule by its neighbors via the Lennard-Jones interactions. The quantities in square brackets, e.g., $[\dot{\varepsilon}]$ or $[\sigma]$, are two-dimensional tensors. T is the temperature of the thermal reservoir, V is the volume of the system (in this case, the area), and N is the number of molecules. T_{kin} is the average kinetic energy per molecule divided by Boltzmann’s constant k_B . $[\sigma]$ is the externally applied stress and $[\sigma_{av}]$ is the average stress throughout the system computed to be

$$[\sigma_{av}]_{ij} = \frac{1}{4V} \sum_n \sum_m F_{nm}^i r_{nm}^j, \quad (2.6)$$

where F_{nm}^i is the i th component of the force between particles n and m , r_{nm}^j is the j th component of the vector displacement between those particles, and V is the volume of the system. \mathbf{L} is the locus of points that describe the boundary of the simulation cell. While Eq. (2.5) is not directly relevant to the dynamics of the particles, keeping track of the boundary is necessary in order to properly calculate intermolecular distances in the periodic cell.

The additional dynamical degrees of freedom in Eqs. (2.1)–(2.5) are a viscosity ξ , which couples the system to the thermal reservoir, and a strain rate $[\dot{\varepsilon}]$, via which the externally applied stress is transmitted to the system. Note that $[\dot{\varepsilon}]$ induces an affine transformation about a reference point \mathbf{R}_0 , which, without loss of generality, we choose to be the origin of our coordinate system. In a conventional formulation, $[\sigma]$ would be equal to $-P[I]$, where P is the pressure and $[I]$ is the unit tensor. In that case, these equations of motion are known to produce the same time-averaged equations of state as an equilibrium NPT ensemble [30]. By instead controlling the tensor $[\sigma]$, including its off-diagonal terms, it is possible to apply a shear stress to the system without creating any preferred surfaces that might enhance system-size effects and interfere with observations of bulk properties. The applied stress and the strain-rate tensor are constrained to be symmetric in order to avoid physically uninteresting rotations of the cell. Except where otherwise noted, all of our numerical experiments are carried out at constant temperature, with $P = 0$, and with the sample loaded in uniform, pure shear.

We have chosen the artificial time constants τ_T and τ_p to represent physical aspects of the system. As suggested by Nose [31], τ_T is the time for a sound wave to travel an interatomic distance and, as suggested by Anderson [36], τ_p is the time for sound to travel the size of the system.

B. Model solid

The special two-component system that we have chosen to study here has been the subject of other investigations [37–39] primarily because it has a quasicrystalline ground state. The important point for our purposes, however, is that

this system can be quenched easily into an apparently stable glassy state. Whether this is actually a thermodynamically stable glass phase is of no special interest here. We care only that the noncrystalline state has a lifetime that is very much longer than the duration of our experiments.

Our system consists of molecules of two different sizes, which we call “small” (*S*) and “large” (*L*). The interactions between these molecules are standard 6-12 Lennard-Jones potentials

$$U_{\alpha\beta}(r) = 4e_{\alpha\beta} \left[\left(\frac{a_{\alpha\beta}}{r} \right)^{12} - \left(\frac{a_{\alpha\beta}}{r} \right)^6 \right], \quad (2.7)$$

where the subscripts α, β denote *S* or *L*. We choose the zero-energy interatomic distances $a_{\alpha\beta}$ to be

$$a_{SS} = 2 \sin\left(\frac{\pi}{10}\right), \quad a_{LL} = 2 \sin\left(\frac{\pi}{5}\right), \quad a_{SL} = 1, \quad (2.8)$$

with bond strengths

$$e_{SL} = 1, \quad e_{SS} = e_{LL} = \frac{1}{2}. \quad (2.9)$$

For computational efficiency, we impose a finite-range cutoff on the potentials in Eq. (2.7) by setting them equal to zero for separation distances r greater than $2.5a_{SL}$. The masses are all taken to be equal. The ratio of the number of large molecules to the number of small molecules is half the golden mean

$$\frac{N_L}{N_S} = \frac{1 + \sqrt{5}}{4}. \quad (2.10)$$

In the resulting system, it is energetically favorable for ten small molecules to surround one large molecule or for five large molecules to surround one small molecule. The highly frustrated nature of this system avoids problems of local crystallization that often occur in two dimensions where the nucleation of single-component crystalline regions is difficult to avoid. As shown by Lançon *et al.* [37], this system goes through something like a glass transition upon cooling from its liquid state. The glass transition temperature is $0.3T_0$, where $k_B T_0 = e_{SL}$. All the simulations reported here have been carried out at a temperature $T = 0.001T_0$, that is, at 0.3% of the glass transition temperature. Thus all of the phenomena to be discussed here take place at a temperature very much lower than the energies associated with the molecular interactions.

In order to start with a densely packed material, we have created our experimental systems by equilibrating a random distribution of particles under high pressure at the low temperature mentioned above. After allowing the system to relax at high pressure, we have reduced the pressure to zero and again allowed the sample to relax. Our molecular-dynamics procedure permits us to relax the system only for times on the order of nanoseconds, which are not long enough for the material to experience any significant amount of annealing, especially at such a low temperature.

We have performed numerical experiments on two different samples, containing 10 000 and 20 000 molecules, respectively. All of the simulation results shown are from the

TABLE I. Sample sizes and elastic constants.

Sample	Molecules	Shear modulus	Bulk modulus	2D Poisson ratio	Young's modulus
1	10 000	9.9	31	0.51	30
2	20 000	16	58	0.57	50

larger of the two samples; the smaller sample has been used primarily to check the reliability of our procedures. We have created each of these samples only once; thus each experiment using either of them starts with precisely the same set of molecules in precisely the same positions. As will become clear, there are both advantages and uncertainties associated with this procedure. On the one hand, we have a very carefully controlled starting point for each experiment. On the other hand, we do not know how sensitive the mechanical properties of our system might be to details of the preparation process, nor do we know whether to expect significant sample-to-sample variations in the molecular configurations. To illustrate these uncertainties, we show the elastic constants of the samples in Table I. The moduli are expressed there in units of e_{SL}/a_{SL}^2 . [Note that the Poisson ratio for a two-dimensional (2D) system has an upper bound of 1 rather than 0.5 as in the three-dimensional case.] The appreciable differences between the moduli of supposedly identical materials tell us that we must be very careful in drawing detailed conclusions from these preliminary results.

C. Simulation results

1. *Macroscopic observations*

In all of our numerical experiments, we have tried simply to mimic conventional laboratory measurements of viscoplastic properties of real materials. The first of these is a measurement of stress at constant strain rate. As we shall see, this supposedly simplest of the experiments is especially interesting and problematic for us because it necessarily probes time-dependent behavior near the plastic yield stress.

Our results for two different strain rates are shown in Fig. 1. The strain rates are expressed in units proportional to the frequency of oscillation about the minimum in the Lennard-Jones potential, specifically, in units of $\omega_0 = (e_{SL}/ma_{SL}^2)^{1/2}$, where m is the particle mass. [The actual frequency for the *SL* potential, in cycles per second, is $(3 \times 2^{1/3}/\pi)\omega_0 \cong 1.2\omega_0$.] As usual, the sample has been kept at constant temperature and at pressure $P = 0$. At low strain, the material behaves in a linearly elastic manner. As the strain increases, the response becomes nonlinear and the material begins to deform plastically. Plastic yielding, that is, the onset of plastic flow, occurs when the strain reaches approximately 0.7%. Note that the stress does not rise smoothly and monotonically in these experiments. We presume that most of this irregularity would average out in larger systems. As we shall see, however, there may also be more interesting dynamical effects at work here.

In all of the other experiments to be reported here, we have controlled the stress on the sample and measured the strain. In the first of these, shown in Fig. 2, we have increased the stress to various different values and then held it constant.

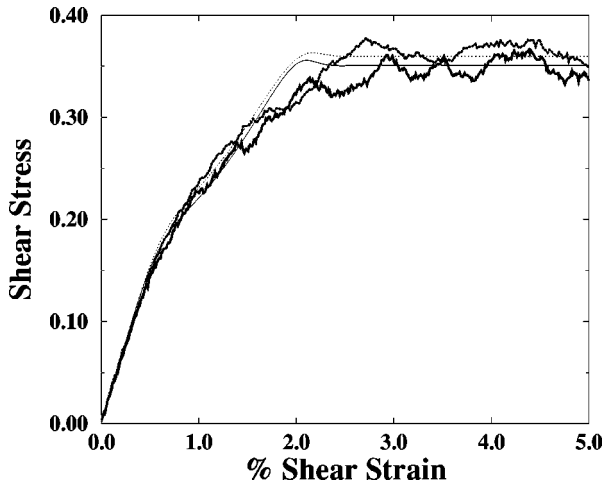


FIG. 1. Shear stress vs strain for strain rates of 10^{-4} (solid lines) and 2×10^{-4} (dotted lines). The thicker lines that denote the simulation results exhibit both linear elastic behavior at low strain and nonlinear response leading to yield at approximately $\sigma_s = 0.35$. The thinner curves are predictions of the theory for the two strain rates. Strain rate is measured in units of $(e_{SL}/m a_{SL}^2)^{1/2}$; stress is measured in units of e_{SL}/a_{SL}^2 .

In each of these experimental runs, the stress starts at zero and increases at the same constant rate until the desired final stress is reached. The graphs show both this applied stress (solid symbols) and the resulting strain (open symbols), as functions of time, for three different cases. Time is measured in the same molecular-vibration units used in the previous experiments, i.e., in units of $(ma_{SL}^2/e_{SL})^{1/2}$. The stresses and strain axes are related by twice the shear modulus so that, if the response is linearly elastic, the two curves lie on top of one another. In the case labeled by triangles, the final stress is small and the response is nearly elastic. For the cases labeled by circles and squares, the sample deforms plasti-

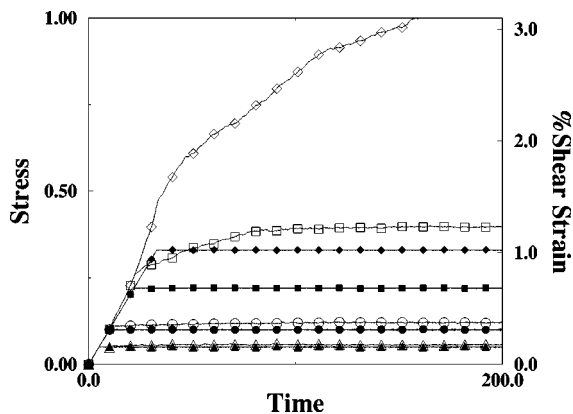


FIG. 2. Shear strain (open symbols) vs time for several applied shear stresses (solid symbols). The stresses have been ramped up at a constant rate until reaching a maximum value and then have been held constant. The strain and stress axes are related by twice the shear modulus so that, for linear elastic response, the open and closed symbols would be coincident. For low stresses the sample responds in an almost entirely elastic manner. For intermediate stresses the sample undergoes some plastic deformation prior to jamming. In the case where the stress is brought above the yield stress, the sample deforms indefinitely. Time is measured in units of $(ma_{SL}^2/e_{SL})^{1/2}$; stress is measured in units of e_{SL}/a_{SL}^2 .

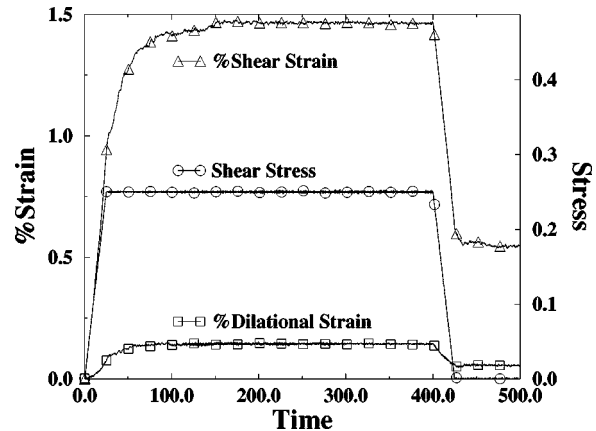


FIG. 3. Stress and strain vs time for one particular loading where the stress has been ramped up to $\sigma_s = 0.25$, held for a time, and then released. Note that, in addition to the shear response, the material undergoes a small amount of dilation. Time is measured in units of $(ma_{SL}^2/e_{SL})^{1/2}$; stress is measured in units of e_{SL}/a_{SL}^2 .

cally until it reaches some final strain, at which it ceases to undergo further deformation on observable time scales. (We cannot rule out the possibility of slow creep at much longer times.) In the case labeled by diamonds, for which the final stress is the largest of the three cases shown, the sample continues to deform plastically at constant stress throughout the duration of the experiment. We conclude from these and a number of similar experimental runs that there exists a well-defined critical stress for this material, below which it reaches a limit of plastic deformation, that is, it ‘jams,’ and above which it flows plastically. Because the stress is ramped up quickly, we can see in curves with squares and diamonds of Fig. 2 that there is a separation of time scales between the elastic and plastic responses. The elastic response is instantaneous, while the plastic response develops over a few hundred molecular vibrational periods. To see the distinction between these behaviors more clearly, we have performed experiments in which we load the system to a fixed, subcritical stress, hold it there, and then unload it by ramping the stress back down to zero. In Fig. 3, we show this stress and the resulting total shear strain, as functions of time, for one of those experiments. If we define the elastic strain to be the stress divided by twice the previously measured, as-quenched, shear modulus, then we can compute the inelastic strain by subtracting the elastic from the total. The result is shown in Fig. 4. Note that most, but not quite all, of the inelastic strain consists of nonrecoverable plastic deformation that persists after unloading to zero stress. Note also, as shown in Fig. 3, that the system undergoes a small dilation during this process and that this dilation appears to have both elastic and inelastic components.

Using the simple prescription outlined above, we have measured the final inelastic shear strain as a function of shear stress. That is, we have measured the shear strain once the system has ceased to deform as in the subcritical cases in Fig. 2, and then subtracted the elastic part. The results are shown in Fig. 5. As expected, we see only very small amounts of inelastic strain at low stress. As the stress approaches the yield stress, the inelastic strain appears to diverge approximately logarithmically.

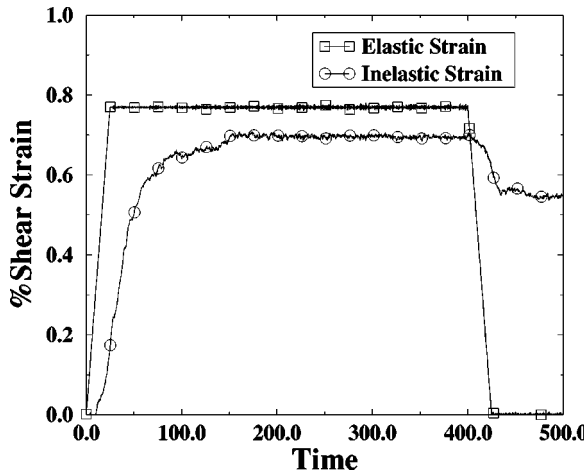


FIG. 4. Elastic and inelastic strain vs time for the same simulation as that shown in Fig. 3. The inelastic strain is found by subtracting the linearly elastic strain from the total strain. Note the partial recovery of the inelastic portion of the strain that occurs during and after unloading. Time is measured in units of $(ma_{SL}^2/e_{SL})^{1/2}$.

The final test that we have performed is to cycle the system through loading, reloading, and reverse loading. As shown in Fig. 6, the sample is first loaded on the curve from *a* to *b*. The initial response is linearly elastic, but, eventually, deviation from linearity occurs as the material begins to deform inelastically. From *b* to *c*, the stress is constant and the sample continues to deform inelastically until reaching a final strain at *c*. Upon unloading, from *c* to *d*, the system does not behave in a purely elastic manner but rather recovers some portion of the strain inelastically. While held at zero stress, the sample continues to undergo inelastic strain recovery from *d* to *e*.

When the sample is then reloaded from *e* to *f*, it undergoes much less inelastic deformation than during the initial loading. From *f* to *g* the sample again deforms inelastically, but by an amount only slightly more than the previously recovered strain, returning approximately to point *c*. Upon unloading again from *g* to *h* to *i*, less strain is recovered than

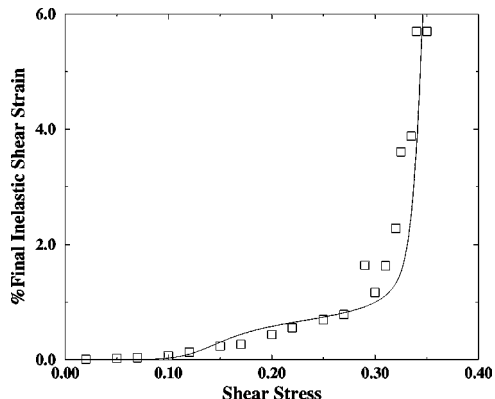


FIG. 5. Final inelastic strain vs applied stress for stresses below yield. The simulation data (squares) have been obtained by running the simulations until all deformation apparently had stopped. The comparison to the theory (line) was obtained by numerically integrating the equations of motion for a period of 800 time units, the duration of the longest simulation runs. Stress is measured in units of e_{SL}/a_{SL}^2 .

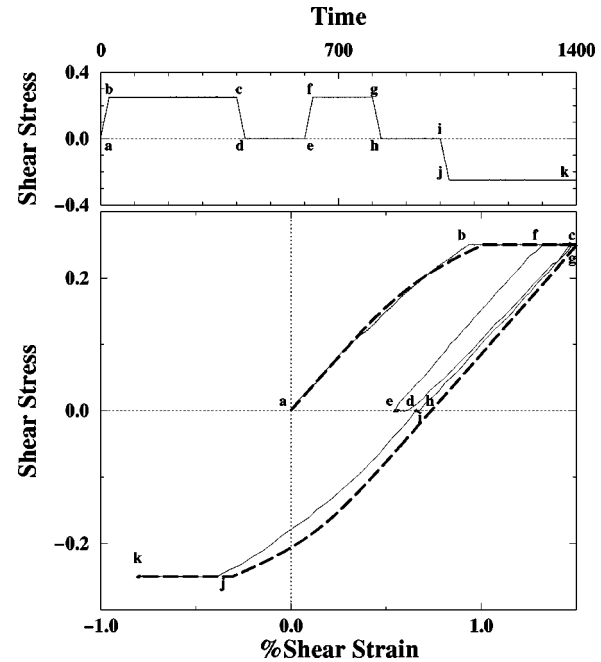


FIG. 6. Stress-strain trajectory for a molecular-dynamics experiment in which the sample has been loaded, unloaded, reloaded, unloaded again, and then reverse loaded, all at stresses below the yield stress. The smaller graph above shows the history of applied shear stress with letters indicating identical times in the two graphs. The dashed line in the main graph is the theoretical prediction for the same sequence of stresses. Note that a small amount of inelastic strain recovery occurs after the first unloading in the simulation, but that no such behavior occurs in the theory. Thus the theoretical curve from *c* through *h* unloads, reloads, and unloads again all along the same line. Time is measured in units of $(ma_{SL}^2/e_{SL})^{1/2}$; stress is measured in units of e_{SL}/a_{SL}^2 .

in the previous unloading from *c* through *e*.

It is during reverse loading from *i* to *k* that it becomes apparent that the deformation history has rendered the amorphous sample highly anisotropic in its response to further applied shear. The inelastic strain from *i* to *k* is much greater than that from *e* to *g*, demonstrating a very significant Bauschinger effect. The plastic deformation in the initial direction apparently has biased the sample in such a way as to inhibit further inelastic yield in the same direction, but there is no such inhibition in the reverse direction. The material, therefore, must in some way have microstructurally encoded, i.e., partially "memorized," its loading history.

2. Microscopic observations

Our numerical methods allow us to examine what is happening at the molecular level during these deformations. To do this systematically, we need to identify where irreversible plastic rearrangements are occurring. More precisely, we must identify places where the molecular displacements are nonaffine, that is, where they deviate substantially from displacements that can be described by a linear strain field.

We start with a set of molecular positions and subsequent displacements and compute the closest possible approximation to a local strain tensor in the neighborhood of any particular molecule. To define that neighborhood, we define a

sampling radius, which we choose to be the interaction range $2.5a_{SL}$. The local strain is then determined by minimizing the mean-square difference between the actual displacements of the neighboring molecules relative to the central one and the relative displacements that they would have if they were in a region of uniform strain ε_{ij} . That is, we define

$$D^2(t, \Delta t) = \sum_n \sum_i \left(r_n^i(t) - r_0^i(t) - \sum_j (\delta_{ij} + \varepsilon_{ij}) \times [r_n^j(t - \Delta t) - r_0^j(t - \Delta t)] \right)^2, \quad (2.11)$$

where the indices i and j denote spatial coordinates and the index n runs over the molecules within the interaction range of the reference molecule, $n=0$ being the reference molecule. $r_n^i(t)$ is the i th component of the position of the n th molecule at time t . We then find the ε_{ij} that minimizes D^2 by calculating

$$X_{ij} = \sum_n [r_n^i(t) - r_0^i(t)] \times [r_n^j(t - \Delta t) - r_0^j(t - \Delta t)], \quad (2.12)$$

$$Y_{ij} = \sum_n [r_n^i(t - \Delta t) - r_0^i(t - \Delta t)] \times [r_n^j(t - \Delta t) - r_0^j(t - \Delta t)], \quad (2.13)$$

$$\varepsilon_{ij} = \sum_k X_{ik} Y_{jk}^{-1} - \delta_{ij}. \quad (2.14)$$

The minimum value of $D^2(t, \Delta t)$ is then the local deviation from affine deformation during the time interval $[t - \Delta t, t]$. We shall refer to this quantity as D_{min}^2 .

We have found that D_{min}^2 is an excellent diagnostic for identifying local irreversible shear transformations. Figure 7 contains four different intensity plots of D_{min}^2 for a particular system as it is undergoing plastic deformation. The stress has been ramped up to $|\sigma_s| = 0.12$ in the time interval $[0, 12]$ and then held constant in an experiment analogous to that shown in Fig. 2. Figure 7(a) shows D_{min}^2 for $t = 10$, $\Delta t = 10$. It demonstrates that the nonaffine deformations occur as isolated small events. In Fig. 7(b) we observe the same simulation, but for $t = 30$, $\Delta t = 30$; that is, we are looking at a later time, but again we consider rearrangements relative to the initial configuration. Now it appears that the regions of rearrangement have a larger scale structure. The pattern seen here looks like an incipient shear band. However, in Fig. 7(c), where $t = 30$, $\Delta t = 1$, we again consider this later time but look only at rearrangements that have occurred in the preceding short time interval. The events shown in this figure are small, demonstrating that the pattern shown in Fig. 7(b) is, in fact, an aggregation of many local events. Finally, in Fig. 7(d), we show an experiment similar in all respects to Fig. 7(a) except that the sign of the stress has been reversed. As in Fig. 7(a), $t = 10$, $\Delta t = 10$, and again we observe small

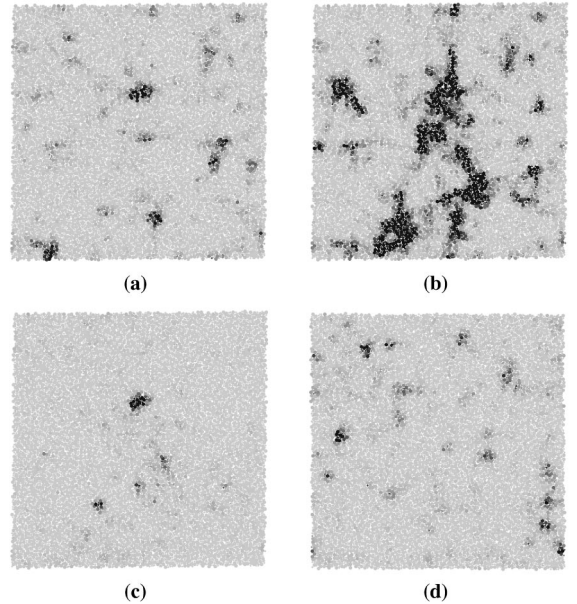


FIG. 7. Intensity plots of D_{min}^2 , the deviation from affine deformation, for various intervals during two simulations. (a)–(c) show deformation during one simulation in which the stress has been ramped up quickly to a value less than the yield stress and then held constant. (a) shows deformations over the first 10 time units and (b) over the first 30 time units. (c) shows the same state as in (b), but with D_{min}^2 computed only for deformations that took place during the preceding 1 time unit. In (d), the initial system and the time interval (10 units) are the same as in (a), but the stress has been applied in the opposite direction. The gray scale in these figures has been selected so that the darkest spots identify molecules for which $|D_{min}| \approx 0.5a_{SL}$.

isolated events. However, these events occur in different locations, implying a direction dependence of the local transformation mechanism.

Next we look at these processes in yet more detail. Figure 8 is a closeup of the molecular configurations in the lower left-hand part of the largest dark cluster seen in Fig. 7(c), shown just before and just after a shear transformation. During this event, the cluster of one large and three small molecules has compressed along the top-left to bottom-right axis and extended along the bottom-left to top-right axis. This deformation is consistent with the orientation of the applied shear, which is in the direction shown by the arrows on the

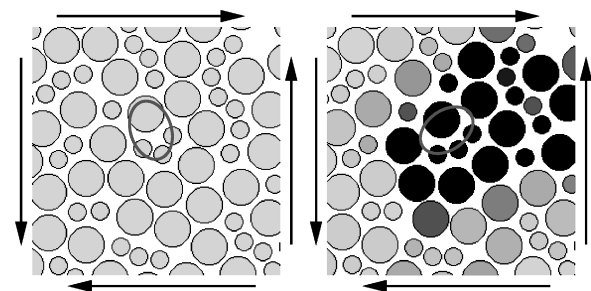


FIG. 8. Closeup picture of a shear transformation zone before and after undergoing transformation. Molecules after transformation are shaded according to their values of D_{min}^2 using the same gray scale as in Fig. 7. The direction of the externally applied shear stress is shown by the arrows. The ovals are included solely as guides for the eye.

outside of the figure. Note that this rearrangement takes place without significantly affecting the relative positions of molecules in the immediate environment of the transforming region. This is the type of rearrangement that Spaepen identifies as a "flow defect" [20]. As mentioned in the Introduction, we shall call these regions shear transformation zones.

III. THEORETICAL INTERPRETATION OF THE MOLECULAR-DYNAMICS EXPERIMENTS

A. Basic hypotheses

We turn now to our attempts to develop a theoretical interpretation of the phenomena seen in the simulations. We shall not insist that our theory reproduce every detail of these results. In fact, the simulations are not yet complete enough to tell us whether some of our observations are truly general properties of the model or are artifacts of the ways in which we have prepared the system and carried out the numerical experiments. Our strategy will be first to specify what we believe to be the basic framework of a theory and then to determine which specific assumptions within this framework are consistent with the numerical experiments.

There are several features of our numerical experiments that we shall assume are fundamentally correct and which, therefore, must be outcomes of our theory. These are the following. (i) At a sufficiently small, fixed load, i.e., under a constant shear stress less than some value that we identify as a yield stress, the system undergoes a finite plastic deformation. The amount of this deformation diverges as the loading stress approaches the yield stress. (ii) At loading stresses above the yield stress, the system flows viscoplastically. (iii) The response of the system to loading is history dependent. If it is loaded, unloaded, and then reloaded to the same stress, it behaves almost elastically during the reloading, i.e., it does not undergo additional plastic deformation. On the other hand, if it is loaded, unloaded, and then reloaded with a stress of the opposite sign, it deforms substantially in the opposite direction.

Our theory consists of a set of rate equations describing plastic deformation. These include an equation for the inelastic strain rate as a function of the stress plus other variables that describe the internal state of the system. We also postulate equations of motion for these state variables. Deformation theories of this type are in the spirit of investigations by Hart [15], who, to the best of our knowledge, was the first to argue in a mathematically systematic way that any satisfactory theory of plasticity must include dynamical state variables, beyond just stress and strain. A similar point of view has been stressed by Rice [16]. Our analysis is also influenced by the use of state variables in theories of friction proposed recently by Ruina, Dieterich, Carlson, and others [40–45].

Our picture of what is happening at the molecular level in these systems is an extension of the ideas of Turnbull, Cohen, Argon, Spaepen, and others [17–21,23–25]. These authors postulated that deformation in amorphous materials occurs at special sites where the molecules are able to rearrange themselves in response to applied stresses. As described in Sec. II, we do see such sites in our simulations and shall use these shear transformation zones as the basis for our analysis. However, we must be careful to state as precisely as possible

our definition of these zones because we shall use them in ways that were not considered by the previous authors.

One of the most fundamental differences between previous work and ours is the fact that our system is effectively at zero temperature. When it is in mechanical equilibrium, no changes occur in its internal state because there is no thermal noise to drive such changes. Thus the shear transformation zones can undergo transitions only when the system is in motion. Because the system is strongly disordered, the forces induced by large-scale motions at the position of any individual molecule may be noisy. These fluctuating forces may even look as if they have a thermal component [46]. The thermodynamic analogy (thermal activation of shear transformations with temperature being some function of the shear rate) may be an alternative to (or an equivalent of) the theory to be discussed here. However, it is beyond the scope of the present investigation.

Our next hypothesis is that shear transformation zones are geometrically identifiable regions in an amorphous solid. That is, we assume that we could, at least in principle, look at a picture of any one of the computer-generated states of our system and identify small regions that are particularly susceptible to inelastic rearrangement. As suggested by Fig. 8, these zones might consist of groups of four or more relatively loosely bound molecules surrounded by more rigid "cages," but that specific picture is not necessary. The main idea is that some such irregularities are locked in on time scales that are very much longer than molecular collision times. That is not to say that these zones are permanent features of the system on experimental time scales. On the contrary, the tendency of these zones to appear and disappear during plastic deformation will be an essential ingredient of our theory.

We suppose further that these shear transformation zones are two-state systems. That is, in the absence of any deformation of the cage of molecules that surrounds them, they are equally stable in either of two configurations. Very roughly speaking, the molecular arrangements in these two configurations are elongated along one or the other of two perpendicular directions, which, shortly, we shall take to be coincident with the principal axes of the applied shear stress. The transition between one such state and the other constitutes an elementary increment of shear strain. Note that bistability is the natural assumption here. More than two states of comparable stability might be possible but would have relatively low probability. A crucial feature of these bistable systems is that they can transform back and forth between their two states but cannot make repeated transformations in one direction. Thus there is a natural limit to how much shear can take place at one of these zones so long as the zone remains intact.

We now consider an ensemble of shear transformation zones and estimate the probability that any one of them will undergo a transition at an applied shear stress σ_s . Because the temperatures at which we are working are so low that ordinary thermal activation is irrelevant, we focus our attention on entropic variations of the local free volume. Our basic assumption is that the transition probability is proportional to the probability that the molecules in a zone have a sufficiently large excess free volume, say, ΔV^* , in which to rearrange themselves. This critical free volume must depend

on the magnitude and orientation of the elastic deformation of the zone that is caused by the externally applied stress σ_s .

At this point, our analysis borrows in its general approach, but not in its specifics, from recent developments in the theory of granular materials [47] where the only extensive state variable is the volume Ω . What follows is a very simple approximation, which, at great loss of generality, leads us quickly to the result that we need. The free volume, i.e., the volume in excess of close packing that the particles have available for motion, is roughly

$$\Omega - Nv_0 \approx Nv_f, \quad (3.1)$$

where N is the total number of particles, v_f is the average free volume per particle, and v_0 is the volume per particle in an ideal state of random dense packing. In the dense solids of interest to us here $v_f \ll v_0$ and therefore v_0 is approximately the average volume per particle even when the system is slightly dilated. The number of states available to this system is roughly proportional to $(v_f/h)^N$, where h is an arbitrary constant with dimensions of volume (the analog of Planck's constant in classical statistical mechanics) that plays no role other than to provide dimensional consistency. Thus the entropy, defined here to be a dimensionless quantity, is

$$S(\Omega, N) \approx N \ln\left(\frac{v_f}{h}\right) \approx N \ln\left(\frac{\Omega - Nv_0}{N h}\right). \quad (3.2)$$

The intensive variable analogous to temperature is χ :

$$\frac{1}{\chi} \equiv \frac{\partial S}{\partial \Omega} \approx \frac{1}{v_f}. \quad (3.3)$$

Our activation factor, analogous to the Boltzmann factor for thermally activated processes, is therefore

$$e^{-(\Delta V^*/\chi)} \approx e^{-(\Delta V^*/v_f)}. \quad (3.4)$$

A formula like Eq. (3.4) appears in various places in the earlier literature [17,23–25]. There is an important difference between its earlier use and the way in which we are using it here. In earlier interpretations, Eq. (3.4) is an estimate of the probability that any given molecule has a large enough free volume near it to be the site at which a thermally activated irreversible transition might occur. In our interpretation, Eq. (3.4) plays more nearly the role of the thermal activation factor itself. It tells us something about the configurational probability for a zone, not just for a single molecule. When multiplied by the density of zones and a rate factor, about which we shall have more to say shortly, it becomes the transformation rate per unit volume.

Note what is happening here. Our system is extremely nonergodic and, even when it is undergoing appreciable strain, does not explore more than a very small part of its configuration space. Apart from the molecular rearrangements that take place during plastic deformation, the only chance that the system has for coming close to any state of equilibrium occurs during the quench by which it is formed initially. Because we control only the temperature and pressure during that quench, we must use entropic considerations to compute the relative probabilities of various molecular configurations that result from it.

The transitions occurring within shear transformation zones are strains and therefore they must, in principle, be described by tensors. For present purposes, however, we can make some simplifying assumptions. As described in Sec. II, our molecular-dynamics model is subject only to a uniform, pure shear stress of magnitude σ_s and a hydrostatic pressure P (usually zero). Therefore, in the principal-axis system of coordinates, the stress tensor is

$$[\sigma] = \begin{bmatrix} -P & \sigma_s \\ \sigma_s & -P \end{bmatrix}. \quad (3.5)$$

Our assumption is that the shear transformation zones are all oriented along the same pair of principal axes and therefore that the strain tensor has the form

$$[\varepsilon] = \begin{bmatrix} \varepsilon_d & \varepsilon_s \\ \varepsilon_s & \varepsilon_d \end{bmatrix}, \quad (3.6)$$

where ε_s and ε_d are the shear and dilational strains, respectively. The total shear strain is the sum of elastic and inelastic components

$$\varepsilon_s = \varepsilon_s^{el} + \varepsilon_s^{in}. \quad (3.7)$$

By definition, the elastic component is the linear response to the stress

$$\varepsilon_s^{el} = \frac{\sigma_s}{2\mu}, \quad (3.8)$$

where μ is the shear modulus.

In a more general formulation, we shall have to consider a distribution of orientations of the shear transformation zones. That distribution will not necessarily be isotropic when plastic deformations are occurring and very likely the distribution itself will be a dynamical entity with its own equations of motion. Our present analysis, however, is too crude to justify any such level of sophistication.

The last of our main hypotheses is an equation of motion for the densities of the shear transformation zones. Denote the two states of the shear transformation zones by the symbols $+$ and $-$ and let n_{\pm} be the number densities of zones in those states. We then write

$$\dot{n}_{\pm} = R_{\mp} n_{\mp} - R_{\pm} n_{\pm} - C_1(\sigma_s \dot{\varepsilon}_s^{in}) n_{\pm} + C_2(\sigma_s \dot{\varepsilon}_s^{in}). \quad (3.9)$$

Here the R_{\pm} are the rates at which \pm states transform to \mp states. These must be consistent with the transition probabilities described in the previous paragraphs.

The last two terms in Eq. (3.9) describe the way in which the population of shear transformation zones changes as the system undergoes plastic deformation. The zones can be annihilated and created, as shown by the terms with coefficients C_1 and C_2 , respectively, at rates proportional to the rate $\sigma_s \dot{\varepsilon}_s^{in}$ at which irreversible work is being done on the system. This last assumption is simple and plausible, but it is not strictly dictated by the physics in any way that we can see. As a caveat we mention that in certain circumstances, when the sample does work on its environment, $\sigma_s \dot{\varepsilon}_s^{in}$ could

be negative, in which case the annihilation and creation terms in Eq. (3.9) could produce results that would not be physically plausible. We believe that such states in our theory are dynamically accessible only from unphysical starting configurations. In related theories, however, that may not be the case.

It is important to recognize that the annihilation and creation terms in Eq. (3.9) are interaction terms and that they have been introduced here in a mean-field approximation. That is, we implicitly assume that the rates at which shear transformation zones are annihilated and created depend only on the rate at which irreversible work is being done on the system as a whole and that there is no correlation between the position at which the work is being done and the place where the annihilation or creation is occurring. This is, in fact, not the case as shown by Fig. 7(b) and is possibly the weakest aspect of our theory. With the preceding definitions, the time rate of change of the inelastic shear strain $\dot{\varepsilon}_s^{in}$ has the form

$$\dot{\varepsilon}_s^{in} = V_z \Delta \varepsilon [R_+ n_+ - R_- n_-], \quad (3.10)$$

where V_z is the typical volume of a zone and $\Delta \varepsilon$ is the increment of local shear strain.

B. Specific assumptions

We turn now to the more detailed assumptions and analyses that we need in order to develop our general hypotheses into a testable theory. According to our hypothesis about the probabilities of volume fluctuations, we should write the transition rates in Eq. (3.9) in the form

$$R_{\pm} = R_0 \exp \left[- \frac{\Delta V^*(\pm \sigma_s)}{v_f} \right]. \quad (3.11)$$

The prefactor R_0 is an as-yet unspecified attempt frequency for these transformations. In writing Eq. (3.11) we have used the assumed symmetry of the system to note that if $\Delta V^*(\sigma_s)$ is the required excess free volume for a $+ \rightarrow -$ transition, then the appropriate free volume for the reverse transition must be $\Delta V^*(-\sigma_s)$. We adopt the convention that a positive shear stress deforms a zone in such a way that it enhances the probability of a $+ \rightarrow -$ transition and decreases the probability of a $- \rightarrow +$ transition. Then $\Delta V^*(\sigma_s)$ is a decreasing function of σ_s .

Before going any further in specifying the ingredients of R_0 , ΔV^* , etc., it is useful to recast the equations of motion in the following form. Define

$$n_{tot} \equiv n_+ + n_-, \quad n_{\Delta} \equiv n_- - n_+, \quad (3.12)$$

and

$$\begin{aligned} \mathcal{C}(\sigma_s) &\equiv \frac{1}{2} \left[\exp \left(- \frac{\Delta V^*(\sigma_s)}{v_f} \right) + \exp \left(- \frac{\Delta V^*(-\sigma_s)}{v_f} \right) \right], \\ \mathcal{S}(\sigma_s) &\equiv \frac{1}{2} \left[\exp \left(- \frac{\Delta V^*(\sigma_s)}{v_f} \right) - \exp \left(- \frac{\Delta V^*(-\sigma_s)}{v_f} \right) \right]. \end{aligned} \quad (3.13)$$

[For convenience, and in order to be consistent with later assumptions, we have suppressed other possible arguments of the functions $\mathcal{C}(\sigma_s)$ and $\mathcal{S}(\sigma_s)$.] Then Eq. (3.11) becomes

$$\dot{\varepsilon}_s^{in} = R_0 V_z \Delta \varepsilon [n_{tot} \mathcal{S}(\sigma_s) - n_{\Delta} \mathcal{C}(\sigma_s)]. \quad (3.14)$$

The equations of motion for n_{Δ} and n_{tot} are

$$\dot{n}_{\Delta} = \frac{2 \dot{\varepsilon}_s^{in}}{V_z \Delta \varepsilon} \left(1 - \frac{\sigma_s n_{\Delta}}{\bar{\sigma} n_{\infty}} \right) \quad (3.15)$$

and

$$\dot{n}_{tot} = \frac{2 \sigma_s \dot{\varepsilon}_s^{in}}{V_z \Delta \varepsilon \bar{\sigma}} \left(1 - \frac{n_{tot}}{n_{\infty}} \right), \quad (3.16)$$

where $\bar{\sigma}$ and n_{∞} are defined by

$$C_1 \equiv \frac{2}{V_z \Delta \varepsilon n_{\infty} \bar{\sigma}}, \quad C_2 \equiv \frac{1}{V_z \Delta \varepsilon \bar{\sigma}}. \quad (3.17)$$

From Eq. (3.16) we see that n_{∞} is the stable equilibrium value of n_{tot} so long as $\sigma_s \dot{\varepsilon}_s^{in}$ remains positive. $\bar{\sigma}$ is a characteristic stress that, in certain cases, turns out to be the plastic yield stress. As we shall see, we need only the above form of the equations of motion to deduce the existence of the plastic yield stress and to compute some elementary properties of the system.

The interesting time-dependent behavior of the system, however, depends sensitively on the as-yet unspecified ingredients of these equations. Consider first the rate factor R_0 . Our zero-temperature hypothesis implies that R_0 should be zero whenever the inelastic shear rate $\dot{\varepsilon}_s^{in}$ and the elastic shear rate $\dot{\varepsilon}_s^{el} = \dot{\sigma}_s/2\mu$ both vanish. Accordingly, we assume that

$$R_0 \equiv \nu^{1/2} [(\dot{\varepsilon}_s^{el})^2 + (\dot{\varepsilon}_s^{in})^2]^{1/4}, \quad (3.18)$$

where ν is a constant that we must determine from the numerical data. Note that ν contains both an attempt frequency and a statistical factor associated with the multiplicity of trajectories leading from one state to the other in an active zone [48].

We can offer only a speculative justification for the right-hand side of Eq. (3.18). The rearrangements that occur during irreversible shear transformations are those in which molecules deviate from the trajectories that they would follow if the system were a continuous medium undergoing affine strain. If we assume that these deviations are diffusive and that the affine deformation over some time interval scales like the strain rate, then the nonaffine transformation rate must scale like the square root of the affine rate. (Diffusive deviations from smooth trajectories have been observed directly in numerical simulations of sheared foams [46], but only in the equivalent of our plastic flow regime.) In Eq. (3.18) we further assume that the elastic and inelastic strain rates are incoherent and thus write the sum of squares within the square brackets. In what follows, we shall not be able to test the validity of Eq. (3.18) with any precision. Most prob-

TABLE II. Values of parameters for comparison to simulation data.

Parameter	Value
$\bar{\sigma}$	0.32
$V_z \Delta \varepsilon n_\infty$	5.7%
ν	50.0
V_0^*/v_f	14.0
$\bar{\mu}$	0.25
$n_{tot}(0)/n_\infty$	2.0

ably, the only properties of importance to us for the present purposes are the magnitude of R_0 and the fact that it vanishes when the shear rates vanish.

Finally, we need to specify the ingredients of ΔV^* and v_f . For ΔV^* we choose the simple form

$$\Delta V^*(\sigma_s) = V_0^* \exp(-\sigma_s/\bar{\mu}), \quad (3.19)$$

where V_0^* is a volume, perhaps of order the average molecular volume v_0 , and $\bar{\mu}$ has the dimensions of a shear modulus. The right-hand side of Eq. (3.19) simply reflects the fact that the free volume needed for an activated transition will decrease if the zone in question is loaded with a stress that coincides with the direction of the resulting strain. We choose the exponential rather than a linear dependence because it makes no sense for the incremental free volume V_0^* to be negative, even for very large values of the applied stresses.

Irreversibility enters the theory via a simple switching behavior that occurs when the σ_s dependence of ΔV^* in Eq. (3.19) is so strong that it converts a negligibly small rate at $\sigma_s=0$ to a large rate at relevant, nonzero values of σ_s . If this happens, then zones that have switched in one direction under the influence of the stress will remain in that state when the stress is removed.

In the formulation presented here, we consider v_f to be constant. This is certainly an approximation; in fact, as seen in Fig. 3, the system dilates during shear deformation. We have experimented with versions of this theory in which the dilation plays a controlling role in the dynamics via variations in v_f . We shall not discuss these versions further because they behaved in ways that were qualitatively different from what we observed in our simulations. The differences arise from feedback between inelastic dilation and flow that occur in these dilational models and apparently not in the simulations. A simple comparison of the quantities involved demonstrates that the assumption that v_f is approximately constant is consistent with our other assumptions. If we assume that the increment in free volume at zero stress must be of order the volume of a small particle $V_0^* \approx v_0 \approx 0.3$ and then look ahead and use our best-fit value for the ratio $V_0^*/v_f \approx 14.0$ (see Sec. III D, Table II), we find $v_f \approx 0.02$. Since the change in free volume due to a dilational strain ε_d is $\Delta v_f = \varepsilon_d/\rho$, where ρ is the number density and $\varepsilon_d < 0.2\%$ for all shear stresses except those very close to yield, it appears that, generally, $\Delta v_f \approx \varepsilon_d v_0 \ll v_f$. Even when $\varepsilon_d = 1\%$, the value observed in our simulations at yield, the

dilational free volume is only about the same as the initial free volume estimated by this analysis.

As a final step in examining the underlying structure of these equations of motion, we make the scaling transformations

$$\frac{2\mu \varepsilon_s^{in}}{\bar{\sigma}} = \mathcal{E}, \quad \frac{n_\Delta}{n_\infty} = \Delta, \quad \frac{n_{tot}}{n_\infty} = \Lambda, \quad \frac{\sigma_s}{\bar{\sigma}} = \Sigma. \quad (3.20)$$

Then we find

$$\dot{\mathcal{E}} = \bar{\mathcal{E}} \mathcal{F}(\Sigma, \Lambda, \Delta), \quad (3.21)$$

$$\dot{\Delta} = 2\mathcal{F}(\Sigma, \Lambda, \Delta)(1 - \Sigma\Delta), \quad (3.22)$$

$$\dot{\Lambda} = 2\mathcal{F}(\Sigma, \Lambda, \Delta)\Sigma(1 - \Lambda), \quad (3.23)$$

where

$$\mathcal{F}(\Sigma, \Lambda, \Delta) = R_0[\Lambda \mathcal{S}(\Sigma) - \Delta \mathcal{C}(\Sigma)] \quad (3.24)$$

and

$$\begin{aligned} \mathcal{C}(\Sigma) &= \frac{1}{2} \left[\exp\left(-\frac{V_0^*}{v_f} e^{-A\Sigma}\right) + \exp\left(-\frac{V_0^*}{v_f} e^{A\Sigma}\right) \right], \\ \mathcal{S}(\Sigma) &= \frac{1}{2} \left[\exp\left(-\frac{V_0^*}{v_f} e^{-A\Sigma}\right) - \exp\left(-\frac{V_0^*}{v_f} e^{A\Sigma}\right) \right]. \end{aligned} \quad (3.25)$$

Here,

$$A \equiv \frac{\bar{\sigma}}{\mu}, \quad \bar{\mathcal{E}} \equiv \frac{2\mu V_z \Delta \varepsilon n_\infty}{\bar{\sigma}}. \quad (3.26)$$

The rate factor in Eq. (3.18) can be rewritten

$$R_0 = \tilde{\nu}^{1/2} (\dot{\Sigma}^2 + \dot{\mathcal{E}}^2)^{1/4}, \quad (3.27)$$

where

$$\tilde{\nu} \equiv \frac{\bar{\sigma}}{2\mu} \nu. \quad (3.28)$$

C. Special steady-state solutions

Although, in general, we must use numerical methods to solve the fully time-dependent equations of motion, we can solve them analytically for special cases in which the stress Σ is held constant. Note that none of the results presented in this subsection, apart from Eq. (3.35), depend on our specific choice of the rate factor R_0 .

There are two specially important steady-state solutions at constant Σ . The first of these is a jammed solution in which $\dot{\mathcal{E}} = 0$, that is, $\mathcal{F}(\Sigma, \Lambda, \Delta)$ vanishes and therefore

$$\Delta = \Lambda \frac{\mathcal{S}(\Sigma)}{\mathcal{C}(\Sigma)} = \Lambda \mathcal{T}(\Sigma), \quad (3.29)$$

where

$$\mathcal{T}(\Sigma) = 1 - 2 \left[1 + \exp\left(2 \frac{V_0^*}{v_f} \sinh(A\Sigma)\right) \right]^{-1}. \quad (3.30)$$

Now suppose that instead of increasing the stress at a finite rate, as we have done in our numerical experiments, we let it jump discontinuously, from zero, perhaps, to its value Σ at time $t=0$. While Σ is constant, Eqs. (3.22) and (3.23) can be solved to yield

$$\frac{1-\Lambda(t)}{1-\Lambda(0)} = \frac{1-\Sigma\Delta(t)}{1-\Sigma\Delta(0)}, \quad (3.31)$$

where $\Lambda(0)$ and $\Delta(0)$ denote the initial values of $\Lambda(t)$ and $\Delta(t)$, respectively. Similarly, we can solve Eqs. (3.21) and (3.22) for $\mathcal{E}(t)$ in terms of $\Delta(t)$ and obtain a relationship between the bias in the population of defects and the change in strain,

$$\mathcal{E}(t) = \mathcal{E}(0) + \frac{\bar{\mathcal{E}}}{2\Sigma} \ln\left(\frac{1-\Sigma\Delta(0)}{1-\Sigma\Delta(t)}\right). \quad (3.32)$$

Combining Eqs. (3.29), (3.31), and (3.32), we can determine the change in strain prior to jamming. That is, for Σ sufficiently small that the following limit exists, we can compute a final inelastic strain \mathcal{E}_f :

$$\mathcal{E}_f \equiv \lim_{t \rightarrow \infty} \mathcal{E}(t) = \mathcal{E}(0) + \frac{\bar{\mathcal{E}}}{2\Sigma} \ln\left(1 + \Sigma \frac{\mathcal{T}(\Sigma)\Lambda(0) - \Delta(0)}{1 - \Sigma\mathcal{T}(\Sigma)}\right). \quad (3.33)$$

The right-hand side of Eq. (3.33), for $\mathcal{E}(0) = \Delta(0) = 0$, should be at least a rough approximation for the inelastic strain as a function of stress as shown in Fig. 5.

The preceding analysis is our mathematical description of how the system jams due to the two-state nature of the shear transformation zones. Each increment of plastic deformation corresponds to the transformation of zones aligned favorably with the applied shear stress. As the zones transform, the bias in their population, i.e., Δ , grows. Eventually, all of the favorably aligned zones that can transform at the given magnitude and direction of the stress have undergone their one allowed transformation, Δ has become large enough to cause \mathcal{F} in Eq. (3.24) to vanish, and plastic deformation comes to a halt.

The second steady state is a plastically flowing solution in which $\dot{\mathcal{E}} \neq 0$ but $\dot{\Delta} = \dot{\Lambda} = 0$. From Eq. (3.22) and (3.23) we see that this condition requires

$$\Delta = \frac{1}{\Sigma}, \quad \Lambda = 1. \quad (3.34)$$

This leads us directly to an equation for the strain rate at constant applied stress,

$$\dot{\mathcal{E}} = \tilde{\nu} \bar{\mathcal{E}}^2 \left[\mathcal{S}(\Sigma) - \frac{1}{\Sigma} \mathcal{C}(\Sigma) \right]^2. \quad (3.35)$$

This flowing solution arises from the nonlinear annihilation and creation terms in Eq. (3.9). In the flowing state, stresses are high enough that shear transformation zones are continuously created. A balance between the rate of zone creation and the rate of transformation determines the rate of deformation.

Examination of Eqs. (3.22) and (3.23) reveals that the jammed solution (3.29) is stable for low stresses, while the flowing solution (3.34) is stable for high stresses. The crossover between the two solutions occurs when both Eqs. (3.29) and (3.34) are satisfied. This crossover defines the yield stress Σ_y , which satisfies the condition

$$\frac{1}{\Sigma_y} = \mathcal{T}(\Sigma_y). \quad (3.36)$$

Note that the argument of the logarithm in Eq. (3.33) diverges at $\Sigma = \Sigma_y$. Note also that, so long as $(2V_0^*/v_f)\sinh(A\Sigma_y) \gg 1$, Eq. (3.36) implies that $\Sigma_y \approx 1$. This inequality is easily satisfied for the parameters discussed in the following subsection. Thus the dimensional yield stress σ_y is approximated accurately by $\bar{\sigma}$ in our original units defined in Eq. (3.20).

D. Parameters of the theory

There are five adjustable system parameters in our theory: $\bar{\sigma}$, $V_z \Delta \varepsilon n_\infty$, ν , V_0^*/v_f , and $\bar{\mu}$. In addition, we must specify initial conditions for \mathcal{E} , Δ , and Λ . For all cases of interest here, $\mathcal{E}(0) = \Delta(0) = 0$. However, $\Lambda(0) = n_{tot}(0)/n_\infty$ is an important parameter that characterizes the as-quenched initial state of the system and remains to be determined.

To test the validity of this theory, we now must find out whether there exists a set of physically reasonable values of these parameters for which the theory accounts for all (or almost all) of the wide variety of time-dependent phenomena seen in the molecular-dynamics experiments. Our strategy has been to start with rough guesses based on our understanding of what these parameters mean and then to adjust these values by trial and error to fit what we believe to be the crucial features of the experiments. We then have used those values of the parameters in the equations of motion to check agreement with other numerical experiments. In adjusting parameters, we have looked for accurate agreement between theory and experiment in low-stress situations where we expect the concentration of active shear transformation zones to be low and we have allowed larger discrepancies near and above the yield stress where we suspect that interactions between the zones may invalidate our mean-field approximation. Our best-fit parameters are shown in Table II.

The easiest parameter to fit should be $\bar{\sigma}$ because it should be very nearly equal to the yield stress. That is, it should be somewhere in the range 0.30–0.35 according to the data shown in Fig. 5. Note that we cannot use Eq. (3.33) to fit the experimental data near the yield point because both the numerical simulations and the theory tell us that the system approaches its stationary state infinitely slowly there. Moreover, we expect interaction effects to be important here. The solid curve in Fig. 5 is the theoretically predicted strain found by integrating the equations of motion for 800 time units, the duration of the longest of the simulation runs. The downward adjustment of $\bar{\sigma}$, from its apparent value of about 0.35 to its best-fit value of 0.32, has been made on the basis of the latter time-dependent calculations plus evidence about the effect of this parameter in other parts of the theory.

Next we consider $V_z \Delta \varepsilon n_\infty$, a dimensionless parameter that corresponds to the amount of strain that would occur if

the density of zones were equal to the equilibrium concentration ($n_{tot}=n_\infty$) and if all the zones transformed in the same direction in unison. Alternatively, if the local strain increment $\Delta\epsilon$ is about unity, then this parameter is the fraction of the volume of the system that is occupied by shear transformation zones. In either way of looking at this quantity, our best-fit value of 5.7% seems sensible.

The parameter ν is a rate that is roughly the product of an attempt frequency and a statistical factor. The only system-dependent quantity with the dimensions of inverse time is the molecular vibrational frequency, which we have seen is of order unity. Our best-fit value of 50 seems to imply that the statistical factor is moderately large, which, in turn, implies that the shear transformation zones are fairly complex, multimolecule structures. Lacking any first-principles theory of this rate factor, however, we cannot be confident about this observation.

Our first rough guess for a value of V_0^*/v_f comes from the assumption that ΔV^* must be about one molecular volume in the absence of an external stress and that v_f is likely to be about a tenth of this. Thus our best-fit value of 14.0 is reassuringly close to what we expected.

The parameter $\bar{\mu}$, a modulus that characterizes the sensitivity of ΔV^* to the applied stress, is especially interesting. Our best-fit value of 0.25 is almost two orders of magnitude smaller than a typical shear modulus for these systems. This means that the shear transformations are induced by relatively small stresses or, equivalently, the internal elastic modes within the zones are very soft. This conclusion is supported quite robustly by our fitting procedure. Alternative assumptions, such as control by variations in the average free volume v_f discussed earlier, produce qualitatively wrong pictures of the time-dependent onset of plastic deformation.

Finally, we consider $\Lambda(0)=n_{tot}(0)/n_\infty$, the ratio of the initial zone density to the equilibrium zone density. This parameter characterizes the transient behavior associated with the initial quench; that is, it determines the as-quenched system's first response to an applied stress. We can learn something about this parameter by looking at later behavior, i.e., the next few segments of a hysteresis loop such as that shown in Fig. 6. If, as is observed there, the loop narrows after the first leg, then we know that there was an excess of shear transformation zones in the as-quenched system and that this excess was reduced in the initial deformation. An initial excess means $\Lambda(0)>1$, consistent with our best-fit value of 2.0.

E. Comparisons between theory and simulations

We now illustrate the degree to which this theory can and cannot account for the phenomena observed in the numerical experiments.

Figure 9 summarizes one of the principal successes of the theory, specifically, its ability to predict the time-dependent onset of plastic deformation over a range of applied stresses below the yield stress. The solid lines in the figure show the shear strains in three different simulations as functions of time. In each simulation the stress is ramped up at the same controlled rate, held constant for a period of time, and then ramped down, again at the same rate. In the lowest curve the stress reaches a maximum of 0.1 in our dimensionless stress

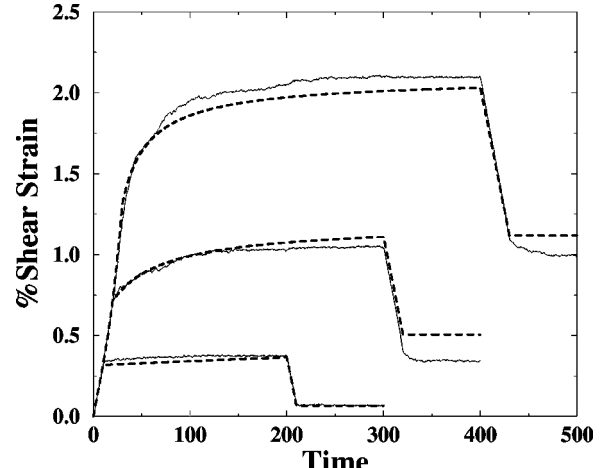


FIG. 9. Strain vs time for simulations in which the stress has been ramped up at a controlled rate to stresses of 0.1, 0.2, and 0.3, held constant, and then ramped down to zero (solid lines). The dashed lines are the corresponding theoretical predictions. Time is measured in units of $(ma_{SL}^2/e_{SL})^{1/2}$.

units (e_{SL}/a_{SL}^2), in the middle curve 0.2, and in the highest 0.3. The dashed lines show the predictions of the theory. The excellent agreement during and after the ramp up is our most direct evidence for the small value of $\bar{\mu}$ quoted above. The detailed shapes of these curves at the tops of the ramps, where $\dot{\sigma}_s$ drops abruptly to zero, provide some qualitative support for our choice of the rate dependence of R_0 in Eq. (3.18). As shown in Fig. 5 and discussed in Sec. III D, the final inelastic strains in these ramp-up experiments are also predicted adequately by the theory.

The situation is different for the unloading phases of these experiments, that is, during and after the periods when the stresses are ramped back down to zero. The theoretical strain rates shown in Fig. 9 vanish abruptly at the bottoms of the ramps because our transformation rates become negligibly small at zero stress. In the two experimental curves for the higher stresses, however, the strain continues to decrease for a short while after the stresses have stopped changing. Our theory seems to rule out any such recovery of inelastic strain at zero stress; thus we cannot account for this phenomenon except to remark that it must have something to do with the initial state of the as-quenched system. As seen in Fig. 6, no such recovery occurs when the system is loaded and unloaded a second time.

In Fig. 6, we compare the stress-strain hysteresis loop in the simulation (solid line) with that predicted by the theory (dashed line). Apart from the inelastic strain recovery after the first unloading in the simulation, the theory and the experiment agree well with one another at least through the reverse loading to point k . The agreement becomes less good in subsequent cycles of the hysteresis loop, possibly because shear bands are forming during repeated plastic deformations.

In the last of the tests of theory to be reported here, we have added in Fig. 1 two theoretical curves for stresses as functions of strain at the two different constant strain rates used in the simulations. The agreement between theory and experiment is better than we probably should expect for situations in which the stresses necessarily rise to values at or

above the yield stress. Moreover, the validity of the comparison is obscured by the large fluctuations in the data, which we believe to be due primarily to small sample size.

Among the interesting features of the theoretical results in Fig. 1 are the peaks in the stresses that occur just prior to the establishment of steady states at constant stresses. These peaks occur because the internal degrees of freedom of the system, specifically $\Delta(t)$ and $\Lambda(t)$, cannot initially equilibrate fast enough to accommodate the rapidly increasing inelastic strain. Thus there is a transient stiffening of the material and a momentary increase in the stress needed to maintain the constant strain rate. This kind of effect may in part be the explanation for some of the oscillations in the stress seen in the experiments. In a more speculative vein, we note that this is our first direct hint of the kind of dynamic plastic stiffening that is needed in order to transmit high stresses to crack tips in brittle fracture. The strain rates near the tips of brittle cracks are at least of the same order of magnitude as the strain rates imposed here and may in fact be substantially higher.

IV. CONCLUDING REMARKS

The most striking and robust conclusion to emerge from this investigation, in our opinion, is that a wide range of realistic, irreversible, viscoplastic phenomena occur in an extremely simple molecular-dynamics model: a two-dimensional, two-component, Lennard-Jones amorphous solid at essentially zero temperature. An almost equally striking conclusion is that a theory based on the dynamics of two-state shear transformation zones is in substantial agreement with the observed behavior of this model. This theory has survived several quantitative tests of its applicability.

We stated in our Introduction that this is a preliminary report. Both the numerical simulations and the theoretical analysis require careful evaluation and improvements. Most importantly, the work so far raises many important questions that need to be addressed in future investigations.

The first kind of question pertains to our molecular-dynamics simulations: Are they accurate and repeatable? We believe that they are good enough for present purposes, but we recognize that there are potentially important difficulties. The most obvious of these is that our simulations have been performed with very small systems; thus size effects may be important. For example, the fact that only a few shear transforming regions are active at any time may account for abrupt jumps and other irregularities sometimes seen in the simulations, e.g., in Fig. 1. We have performed the simulations in a periodic cell to eliminate edge effects. We also have tried to compare results from two systems of different sizes, although only the results from the larger system are presented here. Unfortunately, comparisons between any two different initial configurations are difficult because of our inability, as yet, to create reproducible glassy starting configurations (a problem that we shall discuss next). However, we have seen qualitatively the same behavior in both systems and assume that phenomena that are common to both systems can be used as a guide for theoretical investigations.

As noted in Sec. II B and in Table I, our two systems had quite different elastic moduli. (Remarkably, their yield stresses were nearly identical. It would be interesting to learn

whether this is a repeatable and/or physically important phenomenon.) The discrepancy between the elastic properties of the two systems leads us to believe that, in future work, we shall have to learn how to control the initial configurations more carefully, perhaps by annealing the systems after the initial quenches. Unfortunately, straightforward annealing at temperatures well below the glass transition is not yet possible with standard molecular-dynamics algorithms, which can simulate times only up to about $1 \mu\text{s}$ for systems of this size even with today's fastest computers. Monte Carlo techniques or accelerated molecular-dynamics algorithms may eventually be useful in this effort [49–51]. An alternative strategy may be simply to look at larger numbers of simulations.

By far the most difficult and interesting questions, however, pertain to our theoretical analysis. Although Figs. 7 and 8 provide strong evidence that irreversible shear transformations are localized events, we have no sharp definition of a “shear transformation zone.” So far, we have identified these zones only after the fact, that is, only by observing where the transformations are taking place. Is it possible, at least in principle, to identify zones before they become active?

One ingredient of a better definition of shear transformation zones will be a generalization to isotropic amorphous systems in both two and three dimensions. As we noted in Sec. III, our functions $n_{\pm}(t)$ should be tensor quantities that describe distributions over the ways in which the individual zones are aligned with respect to the orientation of the applied shear stress. We believe that this is a relatively easy generalization; one of us (M.L.F.) expects to report on work along these lines in the future.

Our more urgent reason for needing a better understanding of shear transformation zones is that, without such an understanding, we shall not be able to find first-principles derivations of several, as-yet purely phenomenological, ingredients of our theory. It might be useful, for example, to be able to start from the molecular force constants and calculate the parameters V_0^* and $\bar{\mu}$ that occur in the activation factor (3.19). These parameters, however, seem to have clear physical interpretations; thus we might be satisfied to deduce them from experiment. In contrast, the conceptually most challenging and important terms are the rate factor in Eq. (3.18) and the annihilation and creation terms in Eq. (3.9), where we do not even know what the functional forms ought to be.

Calculating the rate factor in Eq. (3.18), or a correct version of that equation, is clearly a very fundamental problem in nonequilibrium statistical physics. So far as we know, there are no studies in the literature that might help us compute the force fluctuations induced at some site by externally driven deformations of an amorphous material. Nor do we know how to compute a statistical prefactor analogous, perhaps, to the entropic factor that converts an activation energy to an activation free energy. [48] We do know, however, that that entropic factor will depend strongly on the size and structure of the zone that is undergoing the transformation.

As emphasized in Sec. III, the annihilation and creation terms in Eq. (3.9) describe interaction effects. Even within the framework of our mean-field approximation, we do not know with any certainty what these terms should be. Our assumption that they are proportional to the rate of irreversi-

ible work is by no means unique. (Indeed, we have tried other possibilities in related investigations and have arrived at qualitatively similar conclusions.) Without knowing more about the nature of the shear transformation zones, it will be difficult to derive such interaction terms from first principles.

A better understanding of these interaction terms is especially important because these are the terms that will have to be modified when we go beyond the mean-field theory to account for correlations between regions undergoing plastic deformations. We know from our simulations that the active zones cluster even at stresses far below the plastic yield stress and we know that plastic yield in real amorphous materials is dominated by shear banding. Thus, generalizing the present mean-field theory to one that takes into account spatial variations in the densities of shear transformation zones must be a high priority in this research program.

Finally, we return briefly to the question that motivated this investigation: How might the dynamical effects described here, which must occur in the vicinity of a crack tip, control crack stability and brittle or ductile behavior? As we

have seen, our theoretical picture of viscoplasticity does allow large stresses to be transmitted, at least for short times, through plastically deforming materials. It should be interesting to see what happens if we incorporate this picture into theories of dynamic fracture.

ACKNOWLEDGMENTS

This research was supported by DOE Grant No. DE-FG03-84ER45108, by the DOE Computational Sciences Graduate Fellowship Program and, in part, by the MRSEC Program of the National Science Foundation under Grant No. DMR96-32716. We wish particularly to thank Alexander Lobkovsky for his attention to this project and for numerous useful suggestions. We also thank A. Argon and F. Lange for guidance in the early stages of this work, J. Cahn for directing us to the papers of E. Hart, and S. Langer and A. Liu for showing us their closely related results on the dynamics of sheared foams.

-
- [1] J. Langer and A. Lobkovsky, *J. Mech. Phys. Solids* (to be published).
- [2] J. Rice and R. Thomson, *Philos. Mag.* **29**, 73 (1974).
- [3] J. Rice, *J. Mech. Phys. Solids* **40**, 239 (1992).
- [4] M. Khantha, D. Pope, and V. Vitek, *Phys. Rev. Lett.* **73**, 684 (1994).
- [5] L. Freund and Y. Lee, *Int. J. Fract.* **42**, 261 (1990).
- [6] P. Steif, *J. Mech. Phys. Solids* **31**, 359 (1983).
- [7] J. Fineberg, S. Gross, M. Marder, and H. Swinney, *Phys. Rev. Lett.* **67**, 457 (1991).
- [8] J. Fineberg, S. Gross, M. Marder, and H. Swinney, *Phys. Rev. B* **45**, 5146 (1992).
- [9] T.-W. Wu and F. Spaepen, *Philos. Mag. B* **61**, 739 (1990).
- [10] P. Chaudhari, A. Levi, and P. Steinhardt, in *Glassy Metals II*, edited by H. Beck and H.-J. Guntherodt (Springer-Verlag, Berlin, 1983), Vol. 53, p. 127.
- [11] F. Spaepen and A. Taub, in *Amorphous Metallic Alloys*, edited by F. Luborsky (Butterworths, London, 1983), p. 231.
- [12] A. Taub, *Acta Metall.* **30**, 2117 (1982).
- [13] H. Kimura and T. Matsumoto, in *Amorphous Metallic Alloys* (Ref. [11]), p. 187.
- [14] E. Oleinikraux, O. Salamatina, S. Rudnev, and S. Shenogin, *Polym. Sci.* **35**, 1532 (1993).
- [15] E. Hart, *Acta Metall.* **18**, 599 (1970).
- [16] J. Rice, in *Constitutive Equations in Plasticity*, edited by A. Argon (MIT Press, Cambridge, MA, 1975), p. 23.
- [17] F. Spaepen, *Acta Metall.* **25**, 407 (1977).
- [18] A. Argon, *Acta Metall.* **27**, 47 (1979).
- [19] A. Argon and H. Kuo, *Mater. Sci. Eng.* **39**, 101 (1979).
- [20] F. Spaepen and A. Taub, in *Physics of Defects*, edited by J.-P. P. Balian and M. Kleman, 1981 *Les Houches Lectures*, Session XXXV (North-Holland, Amsterdam, 1981), p. 133.
- [21] A. Argon and L. Shi, *Acta Metall.* **31**, 499 (1983).
- [22] V. Khonik and A. Kosilov, *J. Non-Cryst. Solids* **170**, 270 (1994).
- [23] M. Cohen and D. Turnbull, *J. Chem. Phys.* **31**, 1164 (1959).
- [24] D. Turnbull and M. Cohen, *J. Chem. Phys.* **34**, 120 (1961).
- [25] D. Turnbull and M. Cohen, *J. Chem. Phys.* **52**, 3038 (1970).
- [26] D. Deng, A. Argon, and S. Yip, *Philos. Trans. R. Soc. London, Ser. A* **329**, 549 (1989).
- [27] S. Kobayashi, K. Maeda, and S. Takeuchi, *Acta Metall.* **28**, 1641 (1980).
- [28] K. Maeda and S. Takeuchi, *Philos. Mag. A* **44**, 643 (1981).
- [29] D. Srolovitz, V. Vitek, and T. Egami, *Acta Metall.* **31**, 335 (1983).
- [30] S. Melchionna, G. Ciccotti, and B. Holian, *Mol. Phys.* **78**, 533 (1993).
- [31] S. Nose, *J. Chem. Phys.* **81**, 511 (1984).
- [32] S. Nose, *Mol. Phys.* **52**, 255 (1984).
- [33] S. Nose, *Mol. Phys.* **57**, 187 (1986).
- [34] M. Parrinello and A. Rahman, *J. Appl. Phys.* **52**, 7182 (1981).
- [35] M. Parrinello and A. Rahman, *J. Chem. Phys.* **76**, 2662 (1982).
- [36] H. Anderson, *J. Chem. Phys.* **72**, 2384 (1980).
- [37] F. Lançon, L. Billard, and P. Chaudhari, *Europhys. Lett.* **2**, 625 (1986).
- [38] F. Lançon and L. Billard, *J. Phys. (France)* **49**, 249 (1988).
- [39] R. Mikulla, J. Roth, and H.-R. Trebin, *Philos. Mag. B* **71**, 981 (1995).
- [40] J. Dieterich, *Pure Appl. Geophys.* **116**, 790 (1978).
- [41] J. Dieterich, *J. Geophys. Res.* **84**, 2161 (1979).
- [42] J. Rice and A. Ruina, *J. Appl. Mech.* **105**, 343 (1983).
- [43] A. Ruina, *J. Geophys. Res.* **88**, 10 359 (1983).
- [44] J. Dieterich, *PAGEOPH* **143**, 283 (1994).
- [45] J. Carlson and A. Batista, *Phys. Rev. E* **53**, 4153 (1996).
- [46] S. Langer and A. Liu (unpublished).
- [47] A. Mehta and S. F. Edwards, *Physica A* **157**, 1091 (1990).
- [48] J. Langer, *Ann. Phys. (N.Y.)* **54**, 258 (1969).
- [49] G. Barkema and N. Mousseau, *Phys. Rev. Lett.* **77**, 4358 (1996).
- [50] A. Voter, *J. Chem. Phys.* **106**, 4665 (1997).
- [51] A. Voter, *Phys. Rev. Lett.* **78**, 3908 (1997).